Multiparametric Magnetic Resonance Imaging for Predicting Pathological Response After the First Cycle of Neoadjuvant Chemotherapy in Breast Cancer

Xia Li, PhD, Richard G. Abramson, MD,*†‡ Lori R. Arlinghaus, PhD,* Hakmook Kang, PhD,§ Anuradha Bapsi Chakravarthy, MD,‡‖ Vandana G. Abramson, MD,‡¶ Jaime Farley, RN,‡ Ingrid A. Mayer, MD,¶ Mark C. Kelley, MD,‡# Ingrid M. Meszoely, MD,‡# Julie Means-Powell, MD,‡¶ Ana M. Grau, MD,‡# Melinda Sanders, MD,‡** and Thomas E. Yankeelov, PhD*†‡††‡‡§§*

Objectives: The purpose of this study was to determine whether multiparametric magnetic resonance imaging (MRI) using dynamic contrast-enhanced MRI (DCE-MRI) and diffusion-weighted MRI (DWI), obtained before and after the first cycle of neoadjuvant chemotherapy (NAC), is superior to single-parameter measurements for predicting pathologic complete response (pCR) in patients with breast cancer.

Materials and Methods: Patients with stage II/III breast cancer were enrolled in an institutional review board–approved study in which 3-T DCE-MRI and DWI data were acquired before (n = 42) and after 1 cycle (n = 36) of NAC. Estimates of the volume transfer rate (K^{trans}), extravascular extracellular volume fraction (v_e), blood plasma volume fraction (v_p), and the efflux rate constant ($k_{ep} = K^{trans}/v_e$) were generated from the DCE-MRI data using the Extended Tofts-Key model. The apparent diffusion coefficient (ADC) was estimated from the DWI data. The derived parameter k_{ep}/ADC was compared with single-parameter measurements for its ability to predict pCR after the first cycle of NAC.

Results: The k_{ep}/ADC after the first cycle of NAC discriminated patients who went on to achieve a pCR ($P < 0.001$) and achieved a sensitivity, specificity, positive predictive value, and area under the receiver operator curve (AUC) of 0.92, 0.78, 0.69, and 0.88, respectively. These values were superior to the single parameters k_{ep} (AUC, 0.76) and ADC (AUC, 0.82). The AUCs between k_{ep}/ADC and k_{ep} were significantly different on the basis of the bootstrapped 95% confidence intervals (0.018–0.23), whereas the AUCs between k_{ep}/ADC and ADC trended toward significance (−0.11 to 0.24).

Conclusions: The multiparametric analysis of DCE-MRI and DWI was superior to the single-parameter measurements for predicting pCR after the first cycle of NAC.

Key Words: multiparametric MRI, DCE-MRI and DWI, neoadjuvant chemotherapy, breast cancer, treatment response

(*Invest Radiol* 2014;00: 00–00)

Dynamic contrast-enhanced magnetic resonance imaging (DCE-MRI) and diffusion-weighted MRI (DWI) have matured to the point where they are able to provide quantitative and complementary information on tumor status.[1–6] Dynamic contrast-enhanced magnetic resonance imaging involves the serial acquisition of T1-weighted magnetic resonance (MR) images of a tissue of interest before and after an intravenous injection of a paramagnetic contrast agent (CA). As the CA accumulates and then is eliminated, it changes the native relaxation rate of tissue water and, therefore, the measured MR signal intensity. By fitting the resulting signal intensity time course to an appropriate pharmacokinetic model, physiological parameters can be extracted, which relate to tissue perfusion and permeability (K^{trans}, the volume transfer rate), blood plasma volume fraction (v_p), extravascular extracellular volume fraction (v_e), and the efflux rate constant ($k_{ep} = K^{trans}/v_e$). Diffusion-weighted MRI allows for the in vivo measurement of the motion of water in tissue. By applying 2 or more diffusion-sensitizing gradients with different amplitudes, the apparent diffusion coefficient (ADC) can be estimated from the resulting DWI data to describe the rate of water diffusion in cellular tissues. In well-controlled studies, it has been shown that the ADC varies inversely with cell density.[7]

There have been many efforts using DCE-MRI as a surrogate biomarker for assessing and predicting the response of breast tumors to neoadjuvant chemotherapy (NAC).[8–15] For example, Johansen et al[15] measured the relative signal intensity (ie, the mean signal intensity of the second and third dynamic scans relative to the precontrast scan) after a single cycle of NAC and used the technique to predict clinical response and 5-year survival in 24 patients with locally advanced breast cancer. The authors found that the relative signal intensity value was reduced after only 1 cycle of NAC in patients with clinical treatment response ($P = 0.02$). Ah-See et al[12] calculated the changes in pharmacokinetic parameters estimated from DCE-MRI data before and after 2 cycles of treatment and reported that change in K^{trans} was the best predictor of pathologic nonresponse. They showed that the area under the receiver operating characteristic curve (AUC) was 0.93 and that the sensitivity and specificity were 0.94 and 0.82, respectively.[12] Padhani et al[13] found that both tumor size and change in the range of histograms in K^{trans} after 2 cycles of treatment were equally able to predict eventual response (AUC, 0.93 and 0.94, respectively).

Some studies investigating DWI have found that the ADC can separate responders from nonresponders after NAC.[14,16,17] For example, Sharma et al[16] measured the ADC, tumor diameter, and volume at 4 time points during NAC from 56 patients with locally advanced breast cancer and found that ADC had a higher specificity than morphological variables. However, some other studies failed to show a correlation between ADC and treatment response.[18,19]

In more recent studies,[11,17,20–24] investigators have begun to combine DCE-MRI and DWI data to predict response. However, most previous studies reported the ability of both data to monitor or assess treatment response separately and did not show the performance of the combination of DCE-MRI and DWI. The objective of this study was to determine whether a multiparametric combination of DCE-MRI and DWI data can increase the overall accuracy for predicting pathologic complete response (pCR) in patients with breast cancer

Received for publication April 15, 2014; and accepted for publication, after revision, August 14, 2014.

From the *Institute of Imaging Science, †Department of Radiology and Radiological Sciences, ‡the Vanderbilt-Ingram Cancer Center, Departments of §Biostatistics, ‖Radiation Oncology, ¶Medical Oncology, #Surgical Oncology, **Pathology, ††Physics and Astronomy, ‡‡Cancer Biology, and §§Biomedical Engineering, Vanderbilt University, Nashville, TN.

Conflicts of interest and sources of funding: Supported by the National Institutes of Health through NCI R01CA138599, NCI 1U01CA142565, NCI 1U01CA174706, NCI 1P50 098131, NCI P30 CA068485, and NCRR/NIH UL1 RR024975-01 (Vanderbilt CTSA grant) as well as the Kleberg Foundation (support for the imaging program at our institution) and the AUR-GE Radiology Research Academic Fellowship.

The authors report no conflicts of interest.

Reprints: Thomas E. Yankeelov, PhD, Institute of Imaging Science, Vanderbilt University, AA-1105 Medical Center North, 1161 21st Ave S, Nashville, TN 37232–2310. E-mail: thomas.yankeelov@vanderbilt.edu.

ISSN: 0020-9996/14/0000–0000

undergoing NAC. In particular, we hypothesized that the derived measurement k_{ep}/ADC is superior to single-parametric MRI for the prediction of pathologic response to NAC. The eventual clinical goal was to be able to predict, after the first cycle of NAC, which patients will go on to achieve pCR.

MATERIALS AND METHODS

Patient Eligibility and Enrollment

Patients undergoing NAC for high-risk operable breast cancer were eligible for this prospective, institutional review board–approved study. All patients had histologically documented invasive breast cancer at least 1 cm in the longest dimension with a sufficient risk for recurrence to warrant the use of NAC. This risk was determined by the treating oncologist using pretreatment pathologic characteristics including tumor size, nodal status, grade, Ki-67 level, as well as estrogen receptor, progesterone receptor, and human epidermal growth factor receptor 2 (HER2) status as measured through immunohistochemistry. Positivity of HER2 was defined as an immunohistochemical staining score of 3+ or 2+ with an amplification ratio of 2.2 or greater on fluorescence in situ hybridization.[25] Estrogen and progesterone receptor positivity was defined as at least 1% of tumor cells showing positive nuclear staining of any intensity.[26] Receptor status was considered negative if less than 1% of tumor cells showed nuclear staining of any intensity. In addition to tumor characteristics, patient characteristics such as age and menopausal status were used to predict risk for recurrence. The patients provided written informed consent before participating in this study.

Schema

Magnetic resonance imaging was performed before initiating chemotherapy (t_1), after 1 cycle (t_2), and at the conclusion (t_3) of chemotherapy. The NAC regimen was left to the discretion of the treating oncologist on the basis of patient factors such as menopausal status and age as well as tumor characteristics including size, grade, nodal status, and receptor status.

Pathologic Assessment of Response

Several classifications are available to assess pathologic response after NAC. In the National Surgical Adjuvant Breast and Bowel Project B18 trial, pCR was defined as no histologic evidence of invasive tumor cells in the breast. Recently, more complex mathematical determinations of residual tumor burden have been described.[27–31]

Sataloff et al[32] proposed a dual system that separated assessed residual tumor in the primary tumor site and nodes. Given the growing evidence of the importance of residual nodal disease, we elected to use the Sataloff classification, which takes into account both breast and nodal status.[33] Because the aim of our study was to predict, after the first cycle of NAC, who will achieve pCR and who will not at the conclusion of NAC, we classified those who had no invasive tumor in the breast and nodes as a "pCR" and those with any residual invasive cancer in breast and/or nodes as "non-pCR."

MRI Data Acquisition

Magnetic resonance imaging examinations were performed on a Philips 3-T Achieva MR scanner (Philips Healthcare, Best, The Netherlands) and included both DCE-MRI and DWI acquisitions. Before the DCE-MRI acquisition, data for constructing a T1 map were acquired with a radiofrequency-spoiled 3-dimensional gradient echo multiflip angle approach with 10 flip angles from 2 to 20 degrees in 2-degree increments. For the DCE study, each 20-slice set was collected in 16 seconds at 25 time points for just under 7 minutes of dynamic scanning. A catheter placed within an antecubital vein delivered 0.1 mmol/kg (9–15 mL, depending on patient's weight) of gadopentetate dimeglumine, gadolinium-diethylenetriamine pentaacetic acid, (Magnevist, Wayne, NJ) at 2 mL/s (followed by a saline flush) via a power injector (Medrad, Warrendale, PA) after the acquisition of the first 3 dynamic scans (baseline). Diffusion-weighted MRI was acquired with a single-shot spin echo echo planar imaging sequence in 3 orthogonal diffusion encoding directions (x, y, and z). For 14 patients, b = 0 and 500 s/mm^2, repetition time (TR)/echo time (TE) of 2500 milliseconds/45 milliseconds, Δ = 21.4 milliseconds, δ = 10.3 milliseconds, and 10 signal acquisitions were acquired. For 24 patients, b = 0 and 600 s/mm^2, TR/TE of "shortest" (range, 1800–3083 milliseconds/43–60 milliseconds), Δ = 20.7 to 29 milliseconds, δ = 11.4 to 21 milliseconds, and 10 signal acquisitions were acquired. For 4 patients, b = 50 and 600 s/mm^2 for 2 patients, TR/TE of "shortest" (range, 1840–3593 milliseconds/43–60 milliseconds), Δ = 20.6–29 milliseconds, δ = 11.5–21 milliseconds, and 10 signal acquisitions were acquired. Table 1 lists the acquisition parameters for the T1 map, DCE-MRI, and DWI. (The reasons that we used different b values are that data collection occurred over an extended period of time and that there were both hardware and software upgrades during that time. Changes to the diffusion protocol were made to take advantage of these upgrades to improve image quality. The most recent protocol uses b = 0, 50, and 600 s/mm^2 as a compromise between maximizing lesion discrimination and signal-to-noise ratio.[34,35])

We note that subsets of this patient cohort have been included in a number of previous publications that focused on technical DCE-MRI or DWI data acquisition methods[23,36–41] and integrating such data into a predictive mathematical model of tumor growth.[42]

Quantitative Image Analysis

For each patient at each time point, a region of interest (ROI) was manually drawn to completely surround the enhancing tumor as seen on each DCE-MRI tumor slice. The tumor was then defined as the voxels in each ROI displaying a signal intensity increase of greater than 80% after contrast injection. The threshold was calculated as $\left(\left(\overline{S}_{post}-\overline{S}_{pre}\right)/\overline{S}_{pre}\right)\cdot 100$, where $\overline{S}_{post}$ is the averaged postcontrast signal intensity and $\overline{S}_{pre}$ is the average of the 3 precontrast time points. The threshold of 80% was selected because, in a previous study, it yielded the largest concordance correlation coefficient between the longest

TABLE 1. Data Acquisition Parameters

	TR, milliseconds	TE, milliseconds	FOV, mm^2	Acquisition Matrix	Slice Thickness, mm	Slices	Flip Angle, degree
T1 map	7.9	4.6	220 × 220	192 × 192	5	20	2–20
DCE-MRI	7.9	4.6	220 × 220	192 × 192	5	20	20
DWI	Shortest (1840–3593)	Shortest (43–60)	192 × 192	144 × 144	5	12	90

DCE-MRI indicates dynamic contrast-enhanced magnetic resonance imaging; DWI, diffusion-weighted imaging; FOV, field of view; TE, echo time; TR, repetition time.

dimension of the tumor measured on the surgical specimen and the longest dimension measured on the DCE-MRI data just before surgery as reported previously.[38] The DWI data were rigidly registered[43] to the DCE-MRI data, and the tumor ROIs as defined on the DCE-MRI data were then copied to the registered DWI data so that tumor voxels on both data sets were coaligned.

The extended Tofts-Key model was used to estimate 4 physiological parameters from the DCE-MRI data: the volume transfer rate (K^{trans}), blood volume fraction (v_p), extravascular extracellular volume fraction (v_e), and the efflux rate constant ($k_{ep} = K^{trans}/v_e$). The arterial input function (AIF) was a population-averaged AIF constructed from 50 individual AIFs obtained through a semiautomatic AIF tracking algorithm.[44] Voxels for which the extended Tofts-Key model model did not converge or converged to nonphysical values (ie, $K^{trans} > 5.0$ min^{-1}, $v_e > 1.0$, $v_p > 1.0$, or any parameter below 0.0) were set equal to zero and not included in the subsequent analyses.

The ADC maps were calculated with the following equation: $ADC = \ln(S_1/S_2)/(b_2 - b_1)$, where S_1 and S_2 denote the signal acquired with b values of b_1 and b_2, respectively. Voxels for which the model could not fit the data or converged to nonphysical values (ie, ADC > 3.0×10^{-3} mm^2/s or ADC < 0.01×10^{-3} mm^2/s) were set to zero and not included in the subsequent analyses.

At the first 2 time points, longest dimension (LD), mean DCE-MRI parameters, and mean ADC values were computed for each patient and the changes of each parameter between t_1 and t_2 were calculated. The LD was measured from the tumor ROI estimated from the DCE-MRI data; for each slice with tumor voxels, the distance between any 2 voxels was calculated and the maximum distance in all slices was determined as the LD. The mean and change (from baseline to the post–1-cycle time point) of the derived parameter k_{ep}/ADC were also obtained. We hypothesized that the ratio k_{ep}/ADC would represent a more sensitive and specific metric than any single parameter and is therefore superior for predicting treatment response.

Statistical Analysis

All statistical analyses were performed using MATLAB R2012a (The Mathworks, Natick, MA). Receiver operator characteristic (ROC) curve analysis was performed to test the ability of each single-parameter measurement as well as the derived parameter k_{ep}/ADC to predict pCR.[45] "Optimal" cutoff points, sensitivities, specificities, and positive predictive values (PPV) were calculated to satisfy the Youden index; that is, the point on the ROC curve that is farthest from chance and minimizes the overall rate of misclassification.[46] The areas under the curve were estimated using the trapezoidal rule. The nonparametric Wilcoxon rank sum test[47] was also used to detect whether the parameters between the 2 response groups were significantly different.

To investigate whether the AUC of k_{ep}/ADC was significantly different from the AUC of k_{ep} or ADC, the bootstrap method[48] was performed to generate the differences in AUC between k_{ep}/ADC and k_{ep} as well as those between k_{ep}/ADC and ADC with 1000 replicates. The bootstrapped 95% confidence intervals (CIs) for the AUC differences were then estimated.

RESULTS

Clinical Patient Data

Forty-two patients completed scanning at t_1 and 36 patients completed scanning at t_2. The median age of the patients was 46 years (range, 28–67 years). The median time between t_1 and t_2 was 14 days (range, 7–29 days). The median time between the baseline MRI scan and the first cycle of treatment administration was 3 days (range, 0–15 days). Table 2 summarizes the salient features of the study population, the receptor status, and the corresponding treatment regimens for all patients.

At completion of NAC, 14 patients (33.3%) were defined as having achieved pCR. In the patients who did not achieve pCR, the median size of the residual tumor was 1.4 cm (range, 0.3–8 cm).

Representative Imaging Data

The rows of Figure 1 display the K^{trans}, k_{ep}, v_e, v_p, and ADC maps, respectively, superimposed on anatomical T1-weighted images for a representative patient achieving pCR. The numbers under the panels indicate the mean values for each parameter at each time point. The last row of the figure shows the difference image between precontrast and postcontrast DCE-MRI. For this complete responder, both the mean K^{trans} and the mean k_{ep} decreased after 1 cycle of therapy (the changes are −11% and −26%, respectively), whereas the mean values of v_e, v_p, and ADC increased (16%, 2%, and 30%, respectively). Figure 2 displays similar data for a non-pCR patient for which the mean K^{trans}, k_{ep}, and v_e increased by 22%, 15%, and 4%, respectively, after 1 cycle of treatment, whereas v_p and ADC decreased by 20% and 23%, respectively.

Predictive Performance of DCE-MRI and DWI Data at t_1

Table 3 displays the ROC analysis of the pretreatment data (ie, LD, the DCE-MRI parameters, the ADC, and the parameter k_{ep}/ADC) to predict pathologic response. In this table, the cutoff point, sensitivity, specificity, PPV, and AUC are listed for all the parameters. Table 3 shows that the LD and DCE-MRI parameters (K^{trans}, k_{ep}, v_e, v_p, k_{ep}/ADC) all resulted in an AUC less than 0.7. The ADC data yielded a moderate AUC of 0.72, with sensitivity, specificity, and PPV of 0.93, 0.52, and 0.50, respectively, at the cutoff point of 1.2×10^{-3} mm^2/s.

Predictive Performance of Changes in DCE-MRI and DWI From t_1 to t_2

Thirty-six patients were available for analyzing the changes of both the DCE-MRI and ADC data between the pretherapy and post–1 cycle therapy time points. The LD yielded an AUC of 0.67, with a sensitivity, specificity, and PPV of 0.92, 0.48, and 0.48, respectively. Among the 4 DCE-MRI parameters, the change of k_{ep} yielded the best AUC of 0.68, with a sensitivity, specificity, and PPV of 0.83, 0.62, and 0.56, respectively, at the cutoff point of −18.8%. The derived parameter k_{ep}/ADC yielded an AUC, sensitivity, specificity, and PPV of 0.74, 0.83, 0.67, and 0.59, respectively, at the cutoff point of −20.9%. These data are summarized in Table 4.

Predictive Performance of DCE-MRI and DWI at t_2

Both the DCE-MRI data and the ADC data after the first cycle of chemotherapy were available for the 36 patients. Figure 3 displays the ROC curves and the optimal cutoff points for k_{ep}, ADC, and k_{ep}/ADC, respectively. The dotted line shows the ROC curve of k_{ep} alone, with the optimal cutoff point of 0.28 min^{-1} (marked as a triangle), and the dashed line shows the ROC curve for ADC alone, with the optimal point of 1.4 mm^2/s $\times 10^{-3}$ (marked as a star). The solid line displays the ROC curve for k_{ep}/ADC, with the optimal point of 3.32 1/mm^2 (marked as a star). The k_{ep} yielded an AUC, sensitivity, specificity, and PPV of 0.76, 0.83, 0.65, and 0.56, respectively. The ADC yielded an AUC, sensitivity, specificity, and PPV of 0.82, 0.83, 0.67, and 0.59, respectively. The derived parameter k_{ep}/ADC achieved an AUC, sensitivity, specificity, and PPV of 0.88, 0.92, 0.78, and 0.69, respectively. The LD yielded an AUC of only 0.57, with sensitivity, specificity, and PPV of 0.83, 0.42, and 0.42, respectively. These data are summarized in Table 5.

Figure 4 shows boxplots of k_{ep}, ADC, and k_{ep}/ADC for pCRs and non-pCRs. The lines within the boxes denote the median, and the bottom and top edges of the boxes denote the 25th and 75th percentiles, respectively. The medians of k_{ep} for non-pCRs and pCRs were 0.32 min^{-1} and 0.23 min^{-1} ($P = 0.014$), respectively, whereas they were

1.24 $mm^2/s \times 10^{-3}$ and 1.59 $mm^2/s \times 10^{-3}$ for ADC ($P = 0.0019$) as well as 4.32 $1/mm^2$ and 2.63 $1/mm^2$ for k_{ep}/ADC ($P = 0.00032$), respectively.

Figure 5 shows the distributions of the AUC differences between k_{ep}/ADC and k_{ep} as well as those between k_{ep}/ADC and ADC generated by the bootstrap method. The bootstrapped 95% CIs of the AUC differences between k_{ep}/ADC and k_{ep} were 0.018 to 0.23, indicating that the AUCs between k_{ep}/ADC and k_{ep} were significantly different. Although the 95% bootstrap CIs of the AUC differences between

TABLE 2. Clinical Features of the Study Population

Patient No.	Age, y	Treatment Regimens	Receptor Status			Tumor Grade	Excised Tumor Size	Pathologic Response	Surgery
			ER	PR	HER2				
1	50	dd AC × 4 → Taxol × 12	+	+	−	3	0.5	Non-pCR	Mastectomy
2	52	dd Taxotere × 4	+	−	+	3	1.5	Non-pCR	Lumpectomy
3	60	dd AC × 2 → Taxol−Herceptin × 12	+	+	+	1	2.9	Non-pCR	Lumpectomy
4	36	Cisplatin/taxol ± RAD001 × 12*	−	−	−	2	2.9	Non-pCR	Mastectomy
5	48	dd AC × 4 → Taxol × 4	+	+	−	1	1.3	Non-pCR	Lumpectomy
6	43	dd AC × 4 → Taxol × 4	+	+	−	2	2.6	Non-pCR	Mastectomy
7	59	dd AC × 4 → Taxol × 4	+	+	−	2	4.2	Non-pCR	Mastectomy
8	53	Cisplatin/taxol +/−RAD001 × 12	−	−	−	2	1.3	Non-pCR	Lumpectomy
9	35	Trastuzumab + Carboplatin + Ixabepilone × 6	+	+	+	3	1.4	Non-pCR	Lumpectomy
10	28	cisplatin/taxol +/−RAD001 × 12	−	−	−	3	0.8	Non-pCR	Lumpectomy
11	33	AC × 4 → Taxol × 12	+	+	−	3	1.2	Non-pCR	Mastectomy
12	39	AC × 4 → Taxol × 12	+	+	−	1	2.5	Non-pCR	Mastectomy
13	57	AC × 4 → Taxol × 12	−	−	−	3	N/A†	Non-pCR	Progressed with brain mets
14	67	AC × 4 → Taxol/Herceptin × 12	−	−	+	3	1.8	Non-pCR	Lumpectomy
15	45	Cisplatin/taxol +/−RAD001 × 12	−	−	−	3	0.5	Non-pCR	Mastectomy
16	46	Taxotere/Carboplatin/Herceptin × 6	+	+	+	3	0.3	Non-pCR	Mastectomy
17	47	Taxotere × 3 → dd AC × 4	+	+	−	1	8.0	Non-pCR	Mastectomy
18	36	dd AC × 4 → Taxol × 12	+	+	+	2	1.0	Non-pCR	Mastectomy
19	43	cisplatin/taxol +/−RAD001 × 12	−	−	+	3	0.7	Non-pCR	Mastectomy
20	55	dd AC × 4 → Taxol × 10	+	+	−	2	3.5	Non-pCR	Mastectomy
21	58	cisplatin/taxol +/−RAD001 × 12	−	+	−	2	1.7	Non-pCR	Mastectomy
22	36	dd AC × 4 → Taxol × 12	+	+	−	2	2.1	Non-pCR	Lumpectomy
23	43	Cisplatin/taxol +/−RAD001 × 12	−	−	−	3	1.4	Non-pCR	Mastectomy
24	42	cisplatin/taxol +/−RAD001 × 6	+	+	−	2	3.5	Non-pCR	Mastectomy
25	53	dd AC × 4 → Taxol−Herceptin × 7	−	−	+	3	0	pCR	Lumpectomy
26	46	ddTaxotere → AC	−	+	−	3	0	pCR	Mastectomy
27	46	dd AC × 4 → Taxol−Herceptin × 12	−	−	+	2	0	pCR	Mastectomy
28	33	ddAC × 4 → Taxol × 12	−	−	−	3	0	pCR	Mastectomy
29	39	Trastuzumab and Lapatinib × 12	−	−	+	2	0	pCR	Mastectomy
30	46	ddAC × 4 → Taxol × 12	+	−	−	3	0	pCR	Lumpectomy
31	42	Cisplatin/taxol +/−RAD001 × 12	−	−	−	3	0	pCR	Lumpectomy
32	34	ddTaxotere → AC	−	−	−	3	0	pCR	Lumpectomy
33	44	Trastuzumab and Lapatinib × 12	−	−	+	3	0	pCR	Mastectomy
34	37	Cisplatin/taxol +/−RAD001 × 11	−	−	−	3	0	pCR	Mastectomy
35	39	ddAC × 4 → Taxol x 10	−	−	−	3	0	pCR	Lumpectomy
36	48	Taxotere/Carboplatin/Herceptin × 5	−	−	+	3	0	pCR	mastectomy
37	51	ddAC × 4 → Taxol × 12	−	−	−	3	0	pCR	Lumpectomy
38	67	Herceptin/Lapatinib × 12	−	−	+	3	0	pCR	Lumpectomy
39	48	AC × 4 → Taxol/Herceptin × 12	−	−	+	3	0.4	Non-pCR	Lumpectomy
40	65	Herceptin/Lapatinib × 12	−	−	+	3	1.7	Non-pCR	Mastectomy
41	55	ddAC × 4 → Taxol × 12	+	+	−	3	0.9	Non-pCR	Lumpectomy
42	62	Herceptin/Lapatinib × 24	−	−	+	3	0.9	Non-pCR	Mastectomy

*The study is ongoing and we are blinded to the randomization.

†This patient was transferred to another hospital, and the tumor size is not available.

ER indicates estrogen receptor; HER2, human epidermal growth factor receptor 2; pCR, pathologic complete response; PR, progesterone receptor.

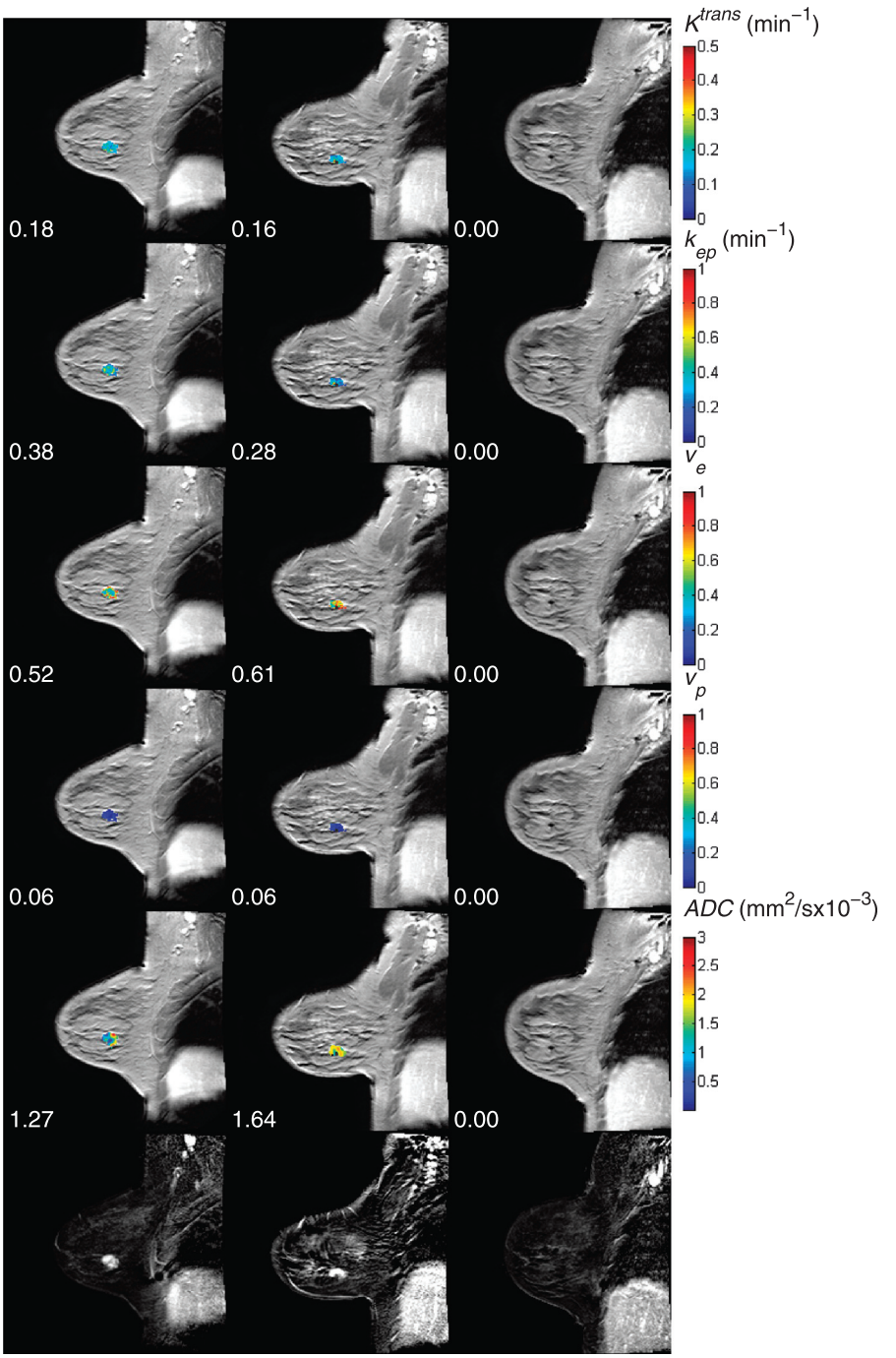

FIGURE 1. The first 5 rows show the K^{trans}, k_{ep}, v_e, v_p, and ADC maps, respectively, superimposed over the postcontrast DCE-MR images at each of the 3 time points (ie, the 3 columns correspond to before treatment, after 1 cycle, and after all cycles of NAC) for 1 patient achieving pCR. The numbers under each panel are the mean values for the parametric map. The last row displays the difference image between precontrast and postcontrast DCE-MRI at each time point.

k_{ep}/ADC and ADC included zero (−0.11 to 0.24), Figure 5 clearly shows a trend approaching significance.

DISCUSSION

To our knowledge, this is the first report of multiparametric quantitative MRI to predict, after the first cycle of NAC, whether patients with breast cancer will achieve pCR at the conclusion of NAC. We chose to study the derived parameter k_{ep}/ADC for statistical and physiological reasons. We reasoned that, in the case of a positive response, k_{ep} would decrease and ADC would increase, whereas in the case of a lack of response, k_{ep} would increase and ADC would decrease. Thus, we hypothesized that the ratio k_{ep}/ADC has the potential to increase the statistical separation between patients going on to achieve pCR versus those who do not (Fig. 4). For this practical reason, the ratio k_{ep}/ADC is a reasonable parameter to consider; indeed, such

derived parameters have been used before, even in the particular case of assessing therapeutic response of breast cancer in the neoadjuvant setting (see, eg, the study of Cerussi et al[49]).

Our results show that the combined parameter k_{ep}/ADC was able to predict pCR with greater accuracy (AUC, 0.88) than did either k_{ep} (AUC, 0.76) or ADC (AUC, 0.82) in isolation. The bootstrap method showed that the AUCs between k_{ep}/ADC and k_{ep} were significantly different and that the AUCs between k_{ep}/ADC and ADC showed a trend approaching significance. Although these results may be considered preliminary owing to our small sample size, we consider them encouraging signs of multiparametric MRI's potential to depict tumor biology and assess therapeutic response early in the course of treatment.[50] Thus, we believe this study contributes to the growing body of knowledge in this developing area.

A secondary finding in this study is that data obtained after the first cycle of therapy were the most statistically robust for predicting

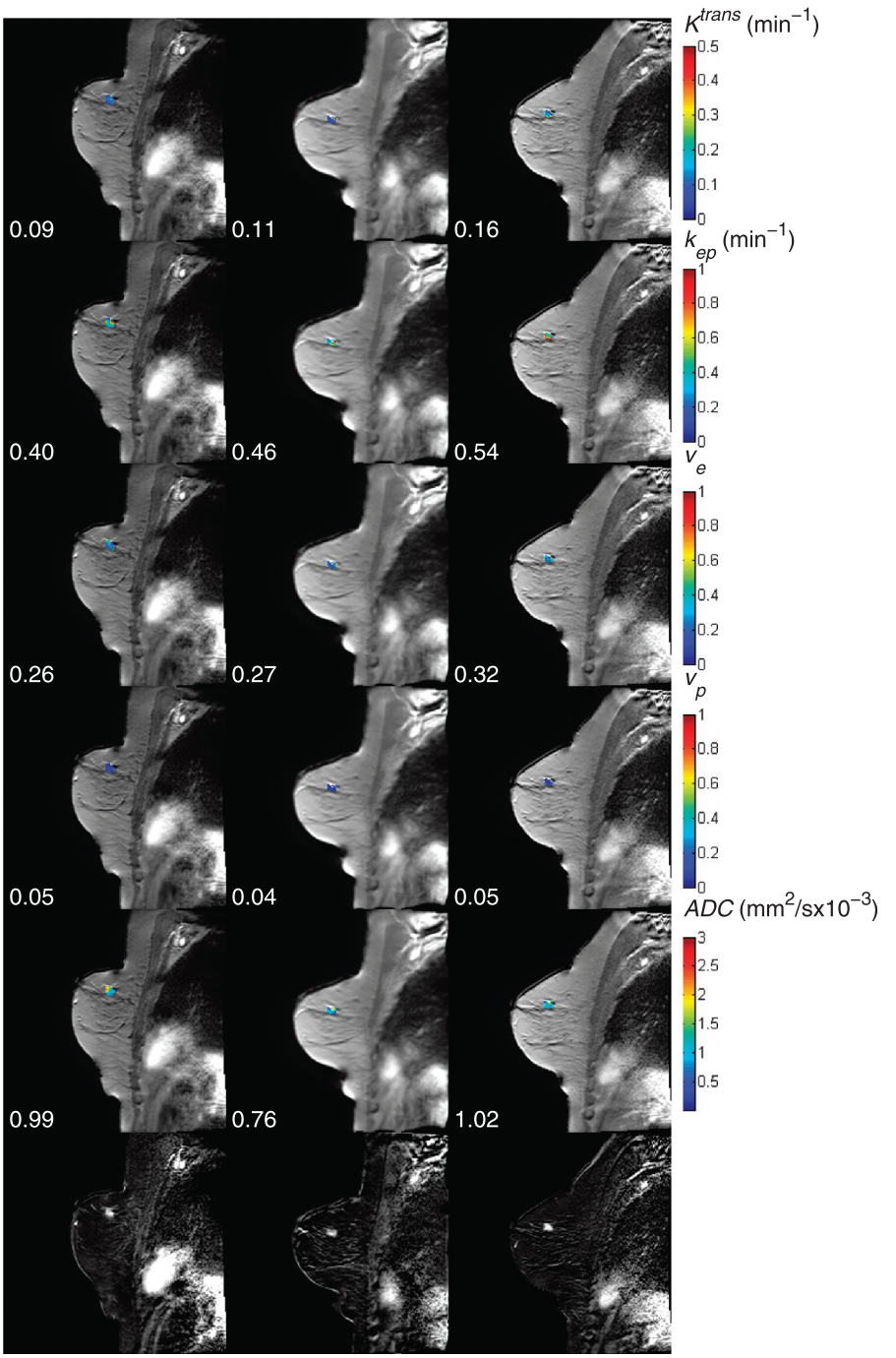

FIGURE 2. The first 5 rows show the K^{trans}, k_{ep}, v_e, v_p, and ADC maps, respectively, superimposed over the postcontrast DCE-MR images at each of the 3 time points (ie, the 3 columns correspond to before treatment, after 1 cycle, and after all cycles of NAC) for 1 non-pCR patient. The numbers under each panel are the mean values for the parametric map. The last row displays the difference image between precontrast and postcontrast DCE-MRI at each time point.

TABLE 3. ROC Analysis of the Parameters at t_1

Parameter	Cutoff	Sensitivity	Specificity	PPV	AUC
LD	3.14 cm	0.86	0.44	0.44	0.63
ADC	1.22×10^{-3} mm^2/s	0.93	0.52	0.50	0.72
K^{trans}	0.08 min^{-1}	0.36	0.88	0.63	0.59
k_{ep}	0.32 min^{-1}	0.79	0.44	0.44	0.53
v_e	0.31	0.29	0.88	0.57	0.51
v_p	0.07	0.93	0.28	0.42	0.53
k_{ep}/ADC	5.18 (1/mm^2)	0.79	0.48	0.46	0.55

ADC indicates apparent diffusion coefficient; AUC, area under the curve; k_{ep}, the efflux rate constant; K^{trans}, the volume transfer rate; LD, longest dimension; PPV, positive predictive value; ROC, receiver operator characteristic; v_e, extravascular extracellular volume fraction; v_p, blood plasma volume fraction.

eventual treatment response. Many previous studies have focused on either pretreatment data or the change between pretreatment data and data acquired after 1 or 2 cycles of chemotherapy.[11–13] Only the study by Fangberget et al[20] reported that the mean ADC values after 4 cycles of NAC showed a significant difference between patients in the pCR and non-pCR groups, whereas the percent change of ADC did not. In our study, we found that the mean parameters of both the DCE-MRI and DWI data after 1 cycle of therapy yielded a better performance (as measured by the ROC analysis) than either the pretreatment data or the percent change of the parameters did.

There are currently few studies that have simultaneously evaluated both DWI and DCE-MRI for predicting the response of breast tumors to NAC[11,17,20,51] and even fewer that have done so after the first cycle of NAC.[52] Furthermore, most of these studies analyzed DWI and DCE-MRI separately and compared their relative predictive abilities, rather than considering their combined utility. Our own group contributed an early hypothesis-generating article on this topic in a small cohort of 11 patients,[11] where we showed that both K^{trans} and ADC were sensitive to longitudinal changes in breast tumor status. Belli et al[17] calculated the longest diameter from contrast-enhanced MRI and the ADC for 51 patients (who received a number of different therapeutic regimens) before and after all cycles of NAC. They reported that the change in the longest diameter accurately evaluated response after NAC with an AUC, sensitivity, specificity, and accuracy of 0.87, 96%, 73%, and 84%, whereas ADC returned values of 0.80, 80%, 84%, and 82%, respectively. Importantly, for the longest diameter, the investigators defined "responders" as those who have a complete response or partial response on the basis of Response Evaluation Criteria in Solid Tumors,[53–55] whereas for the ADC analysis, the investigators

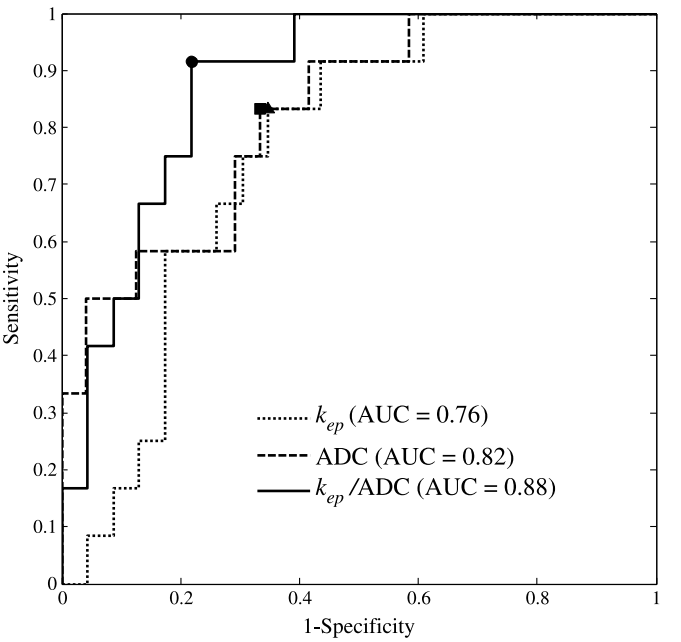

FIGURE 3. The ROC analysis for k_{ep} (dotted line), ADC (dashed line), and k_{ep}/ADC (solid line). Individually, k_{ep} and ADC yielded AUC values of 0.76 and 0.82, respectively, whereas k_{ep}/ADC had an AUC of 0.88. The corresponding optimal cutoff points are also marked by the triangle (k_{ep}), square (ADC), and circle (k_{ep}/ADC). The sensitivity, specificity, and PPV at the cutoff points are 0.83, 0.65, and 0.56 for k_{ep}; 0.83, 0.67, and 0.59 for ADC; and 0.92, 0.78, and 0.69 for k_{ep}/ADC, respectively.

defined "responders" as those who had complete regression, presence of rare cancer cells within fibrotic tissue, or an increase in the number of residual cancer cells provided that fibrosis still dominated the tissue. (Note that this is a markedly different definition of response than that used in the present study.) Fangberget et al[20] assessed ADC, tumor size from contrast-enhanced MRI, and changes in tumor size for 31 patients (also receiving different NAC regimens) before treatment, after 4 cycles, and after all cycles of NAC. The authors showed that the ADC yielded a sensitivity and specificity of 88% and 80%, whereas the tumor volume reduction yielded 91% and 80%, respectively, after 4 cycles of NAC. Hahn et al[51] evaluated the longest diameter from DCE-MRI, DWI, and DCE-MRI plus DWI for 78 patients (also receiving different NAC regimens) before and after all cycles of NAC. Different NAC regimens were assigned according to the receptor status of the biopsied specimen. The investigators simultaneously evaluated the DCE-MRI and DWI

TABLE 4. ROC Analysis of Parameter Changes From t_1 to t_2

Parameter	Cutoff	Sensitivity	Specificity	PPV	AUC
LD	−1.5%	0.92	0.48	0.48	0.67
ADC	6.5%	0.50	0.78	0.55	0.63
K^{trans}	12.7%	1.00	0.33	0.46	0.57
k_{ep}	−18.8%	0.83	0.62	0.56	0.68
v_e	11.9%	0.67	0.76	0.62	0.60
v_p	75.0%	1.00	0.29	0.44	0.55
k_{ep}/ADC	−20.9%	0.83	0.67	0.59	0.74

ADC indicates apparent diffusion coefficient; AUC, area under the curve; k_{ep}, the efflux rate constant; K^{trans}, the volume transfer rate; LD, longest dimension; PPV, positive predictive value; ROC, receiver operator characteristic; v_e, extravascular extracellular volume fraction; v_p, blood plasma volume fraction.

TABLE 5. ROC Analysis of the Parameters at t_2

Parameter	Cutoff	Sensitivity	Specificity	PPV	AUC
LD	1.94 cm	0.83	0.42	0.42	0.57
ADC	1.4×10^{-3} mm^2/s	0.83	0.67	0.59	0.82
K^{trans}	0.1 min^{-1}	0.67	0.74	0.57	0.68
k_{ep}	0.28 min^{-1}	0.83	0.65	0.56	0.76
v_e	0.41	0.67	0.48	0.40	0.54
v_p	0.04	0.50	0.78	0.55	0.61
k_{ep}/ADC	3.32 1/mm^2	0.92	0.78	0.69	0.88

ADC indicates apparent diffusion coefficient; AUC, area under the curve; k_{ep}, the efflux rate constant; K^{trans}, the volume transfer rate; LD, longest dimension; PPV, positive predictive value; ROC, receiver operator characteristic; v_e, extravascular extracellular volume fraction; v_p, blood plasma volume fraction.

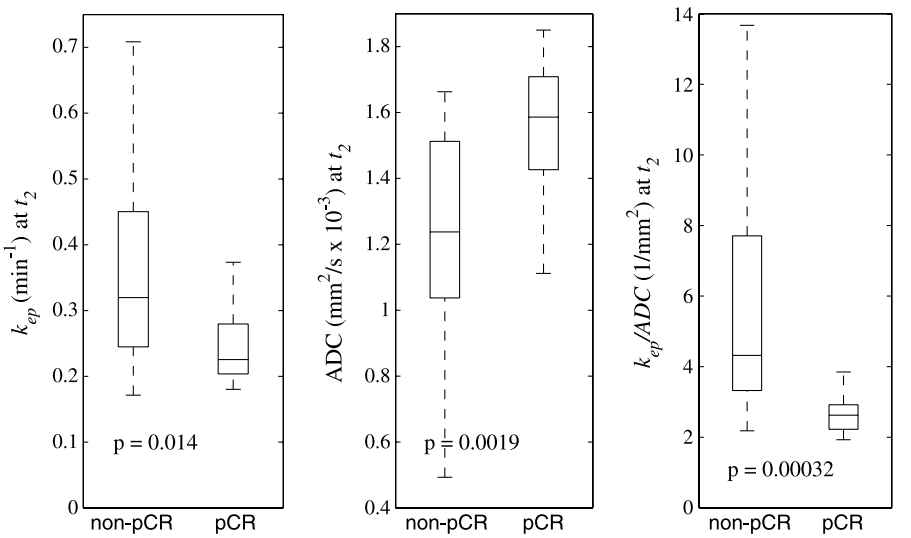

FIGURE 4. Boxplots of k_{ep} (left panel), ADC (middle panel), and k_{ep}/ADC (right panel) at t_2 for non-pCR and pCR patients. The central marks show the median, and the edges of the box are the 25th and 75th percentiles. The medians of k_{ep} for non-pCRs and pCRs were 0.32 min^{-1} and 0.23 min^{-1}, respectively, whereas they were 1.24 mm^2/s $\times$ 10^{-3} and 1.59 mm^2/s $\times$ 10^{-3} for ADC as well as 4.32 1/mm^2 and 2.63 1/mm^2 for k_{ep}/ADC, respectively.

data to measure the longest diameter on both the abnormally enhancing lesions with concurrent high signal intensity on DWI. Using this approach, they reported an improved ability for detecting residual cancer with a sensitivity, specificity, accuracy, PPV, and negative predictive value of 94.8%, 80.0%, 91.0%, 93.2%, and 84.2%, respectively, compared with DCE-MRI alone (91.4%, 45.0%, 79.5%, 82.8%, and 64.3%, respectively) and DWI alone (91.4%, 65.0%, 84.6%, 88.3%, and 72.2%, respectively).

To date, there is only a single (pilot) study that assessed changes in quantitative DCE-MRI and DWI after the first cycle of NAC. Jensen et al[52] assessed tumor diameter and volume, ADC, K^{trans}, and v_e for 15 patients receiving different treatment regimens, 12 of whom were scanned both before and after the first cycle of NAC. For each parameter, a logistic regression analysis with leave-one-out cross-validation was performed. They found that the best predictor for treatment response was a change in tumor diameter with 2 of 12 misclassified patients. The mean change of the longest diameters for the responders was −13% versus −5% for the nonresponders ($P = 0.29$).

The results of the present study are of clinical relevance for a number of reasons. Accurate early assessment of therapeutic response would provide the opportunity to replace an ineffective treatment with an alternative regimen, potentially avoiding or curtailing debilitating adverse effects or toxicities. Patients proven at an early stage to be refractory to multiple NAC regimens could be referred directly to surgery. Techniques for early response assessment will also be important for response-adaptive clinical trials, in which there is growing interest.[56] In light of the current literature (briefly reviewed previously), our results provide compelling motivation for continuing to apply integrated DCE-MRI and DWI to the problem of predicting the eventual response of patients with breast cancer early in the course of NAC. Importantly, the integrated DCE-MRI and DWI approach outperformed the results achieved by the longest diameter size measurement, which is, of course, the basis of Response Evaluation Criteria in Solid Tumors. The current criterion standard for response prediction in the neoadjuvant setting for breast cancer is the I-SPY trial,[57] which achieved an area under the ROC of 0.73 for early prediction of pCR. Thus, our methods compare well with the current state-of-the-art.

There are several limitations of this study. First, the temporal resolution of 16 seconds is not optimal for characterizing the AIF, and this can confound a quantitative DCE-MRI analysis. This temporal resolution was chosen as a compromise between temporal and spatial resolution and field of view coverage (please refer to the study of Li et al[38] for an in-depth discussion). Second, a population AIF was used to estimate the DCE-MRI parameters. In practice, it is difficult to estimate reliable AIFs at each scanning session for each patient. Hence, we used a population AIF as an alternative approach. Third, the patient population received a number of different treatment regimens and it is certainly possible that the imaging biomarkers could vary by both the biology of the disease as well as the agents used. However, current studies[58,59] have a disagreement over the treatment effect on the ability of MRI to predict treatment response. Hence, this is an important area for further study. Another limitation is the modest sample size in our study (data were available on 42 patients before NAC, whereas we were able to acquire data on

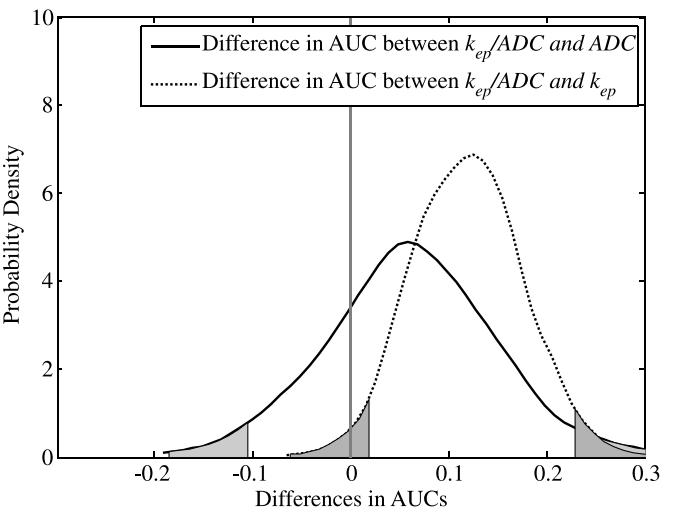

FIGURE 5. The figure displays density distributions of the AUC differences between k_{ep}/ADC and k_{ep} (dotted line) and those between k_{ep}/ADC and ADC (solid line) after 1 cycle of NAC. The 95% CIs of the AUC differences between k_{ep}/ADC and k_{ep} were 0.018 to 0.23, whereas the 95% CIs of the AUC differences between k_{ep}/ADC and ADC were –0.11 to 0.24. The areas outside the 95% CIs are shadowed for both distributions and indicate that the AUCs between k_{ep}/ADC and k_{ep} were significantly different (zero is included in the shadowed area).

36 patients both before and after 1 cycle of NAC). Our findings are thus of a preliminary nature and will need to be validated in larger prospective trials.

In summary, our study shows that combining DCE-MRI and DWI data into a single derived multiparametric measurement k_{ep}/ADC can increase the ability to predict breast cancer response to NAC at a very early time point. It may allow clinicians to tailor therapy on an individual basis. Future work will include investigating multivariate analysis of DCE-MRI and DWI on a larger cohort of patients.

ACKNOWLEDGMENTS

The authors thank the patients and their families for participating in our studies.

REFERENCES

1. Yankeelov TE, Arlinghaus LR, Li X, et al. The role of magnetic resonance imaging biomarkers in clinical trials of treatment response in cancer. *Semin Oncol*. 2011;38:16–25.
2. Pinker K, Bickel H, Helbich TH, et al. Combined contrast-enhanced magnetic resonance and diffusion-weighted imaging reading adapted to the "Breast Imaging Reporting and Data System" for multiparametric 3-T imaging of breast lesions. *Eur Radiol*. 2013;23:1791–1802.
3. Pinker K, Grabner G, Bogner W, et al. A combined high temporal and high spatial resolution 3 Tesla MR imaging protocol for the assessment of breast lesions: initial results. *Invest Radiol*. 2009;44:553–558.
4. Bogner W, Gruber S, Pinker K, et al. Diffusion-weighted MR for differentiation of breast lesions at 3.0 T: how does selection of diffusion protocols affect diagnosis? *Radiology*. 2009;253:341–351.
5. Pinker K, Bogner W, Baltzer P, et al. Improved diagnostic accuracy with multiparametric magnetic resonance imaging of the breast using dynamic contrast-enhanced magnetic resonance imaging, diffusion-weighted imaging, and 3-dimensional proton magnetic resonance spectroscopic imaging. *Invest Radiol*. 2014;49:421–430.
6. Bogner W, Pinker-Domenig K, Bickel H, et al. Readout-segmented echo-planar imaging improves the diagnostic performance of diffusion-weighted MR breast examinations at 3.0 T. *Radiology*. 2012;263:64–76.
7. Guo Y, Cai YQ, Cai ZL, et al. Differentiation of clinically benign and malignant breast lesions using diffusion-weighted imaging. *J Magn Reson Imaging*. 2002; 16:172–178.
8. Cheung YC, Chen SC, Su MY, et al. Monitoring the size and response of locally advanced breast cancers to neoadjuvant chemotherapy (weekly paclitaxel and epirubicin) with serial enhanced MRI. *Breast Cancer Res Treat*. 2003;78:51–58.
9. Chou CP, Wu MT, Chang HT, et al. Monitoring breast cancer response to neoadjuvant systemic chemotherapy using parametric contrast-enhanced MRI: a pilot study. *Acad Radiol*. 2007;14:561–573.
10. Martincich L, Montemurro F, De Rosa G, et al. Monitoring response to primary chemotherapy in breast cancer using dynamic contrast-enhanced magnetic resonance imaging. *Breast Cancer Res Treat*. 2004;83:67–76.
11. Yankeelov TE, Lepage M, Chakravarthy A, et al. Integration of quantitative DCE-MRI and ADC mapping to monitor treatment response in human breast cancer: initial results. *Magn Reson Imaging*. 2007;25:1–13.
12. Ah-See ML, Makris A, Taylor NJ, et al. Early changes in functional dynamic magnetic resonance imaging predict for pathologic response to neoadjuvant chemotherapy in primary breast cancer. *Clin Cancer Res*. 2008;14:6580–6589.
13. Padhani AR, Hayes C, Assersohn L, et al. Prediction of clinicopathologic response of breast cancer to primary chemotherapy at contrast-enhanced MR imaging: initial clinical results. *Radiology*. 2006;239:361–374.
14. Pickles MD, Gibbs P, Lowry M, et al. Diffusion changes precede size reduction in neoadjuvant treatment of breast cancer. *Magn Reson Imaging*. 2006;24:843–847.
15. Johansen R, Jensen LR, Rydland J, et al. Predicting survival and early clinical response to primary chemotherapy for patients with locally advanced breast cancer using DCE-MRI. *J Magn Reson Imaging*. 2009;29:1300–1307.
16. Sharma U, Danishad KK, Seenu V, et al. Longitudinal study of the assessment by MRI and diffusion-weighted imaging of tumor response in patients with locally advanced breast cancer undergoing neoadjuvant chemotherapy. *NMR Biomed*. 2009;22:104–113.
17. Belli P, Costantini M, Ierardi C, et al. Diffusion-weighted imaging in evaluating the response to neoadjuvant breast cancer treatment. *Breast J*. 2011;17:610–619.
18. Woodhams R, Kakita S, Hata H, et al. Identification of residual breast carcinoma following neoadjuvant chemotherapy: diffusion-weighted imaging—comparison with contrast-enhanced MR imaging and pathologic findings. *Radiology*. 2010; 254:357–366.
19. Nilsen L, Fangberget A, Geier O, et al. Diffusion-weighted magnetic resonance imaging for pretreatment prediction and monitoring of treatment response of patients with locally advanced breast cancer undergoing neoadjuvant chemotherapy. *Acta Oncol*. 2010;49:354–360.
20. Fangberget A, Nilsen LB, Hole KH, et al. Neoadjuvant chemotherapy in breast cancer-response evaluation and prediction of response to treatment using dynamic contrast-enhanced and diffusion-weighted MR imaging. *Eur Radiol*. 2011;21: 1188–1199.
21. Wu LM, Hu JN, Gu HY, et al. Can diffusion-weighted MR imaging and contrast-enhanced MR imaging precisely evaluate and predict pathological response to neoadjuvant chemotherapy in patients with breast cancer? *Breast Cancer Res Treat*. 2012;135:17–28.
22. Boehler T, Schilling K, Bick U, et al. Deformable Image Registration of Follow-Up Breast Magnetic Resonance Images. In: Fischer B, Dawant BM, Lorenz C, eds. Verlag Berlin: Springer; 2010:1258–1270.
23. Mani S, Chen Y, Li X, et al. Machine learning for predicting the response of breast cancer to neoadjuvant chemotherapy. *J Am Med Inform Assoc*. 2013;20:688–695.
24. Moestue SA, Huuse EM, Lindholm EM, et al. Low-molecular contrast agent dynamic contrast-enhanced (DCE)-MRI and diffusion-weighted (DW)-MRI in early assessment of bevacizumab treatment in breast cancer xenografts. *J Magn Reson Imaging*. 2013;38:1043–1053.
25. Wolff AC, Hammond ME, Hicks DG, et al. Recommendations for human epidermal growth factor receptor 2 testing in breast cancer: American Society of Clinical Oncology/College of American Pathologists clinical practice guideline update. *J Clin Oncol*. 2013;31:3997–4013.
26. Hammond ME, Hayes DF, Dowsett M, et al. American Society of Clinical Oncology/College Of American Pathologists guideline recommendations for immunohistochemical testing of estrogen and progesterone receptors in breast cancer. *J Clin Oncol*. 2010;28:2784–2795.
27. Wolmark N, Wang J, Mamounas E, et al. Preoperative chemotherapy in patients with operable breast cancer: nine-year results from National Surgical Adjuvant Breast and Bowel Project B-18. *J Natl Cancer Inst Monogr*. 2001;30:96–102.
28. Fisher B, Bryant J, Wolmark N, et al. Effect of preoperative chemotherapy on the outcome of women with operable breast cancer. *J Clin Oncol*. 1998;16: 2672–2685.
29. Symmans WF, Peintinger F, Hatzis C, et al. Measurement of residual breast cancer burden to predict survival after neoadjuvant chemotherapy. *J Clin Oncol*. 2007;25:4414–4422.
30. MD Anderson Residual Cancer Burden Calculator. Available at: http://www3.mdanderson.org/app/medcalc/index.cfm?pagename=jsconvert3. Accessed October 24, 2012.
31. Corben AD, Abi-Raad R, Popa I, et al. Pathologic response and long-term follow-up in breast cancer patients treated with neoadjuvant chemotherapy: a comparison between classifications and their practical application. *Arch Pathol Lab Med*. 2013;137:1074–1082.
32. Sataloff DM, Mason BA, Prestipino AJ, et al. Pathologic response to induction chemotherapy in locally advanced carcinoma of the breast: a determinant of outcome. *J Am Coll Surg*. 1995;180:297–306.
33. Penault-Llorca F, Abrial C, Raoelfils I, et al. Comparison of the prognostic significance of Chevallier and Sataloff's pathologic classifications after neoadjuvant chemotherapy of operable breast cancer. *Hum Pathol*. 2008;39:1221–1228.
34. Chen X, He XJ, Jin R, et al. Conspicuity of breast lesions at different b values on diffusion-weighted imaging. *BMC Cancer*. 2012;12:334.
35. Pereira FP, Martins G, Figueiredo E, et al. Assessment of breast lesions with diffusion-weighted MRI: comparing the use of different b values. *AJR Am J Roentgenol*. 2009;193:1030–1035.
36. Arlinghaus LR, Welch EB, Chakravarthy AB, et al. Motion correction in diffusion-weighted MRI of the breast at 3T. *J Magn Reson Imaging*. 2011;33: 1063–1070.
37. Abramson RG, Li X, Hoyt TL, et al. Early assessment of breast cancer response to neoadjuvant chemotherapy by semi-quantitative analysis of high-temporal resolution DCE-MRI: preliminary results. *Magn Reson Imaging*. 2013;31:1457–1464.
38. Li X, Arlinghaus LR, Ayers GD, et al. DCE-MRI analysis methods for predicting the response of breast cancer to neoadjuvant chemotherapy: pilot study findings. *Magn Reson Med*. 2014;71:1592–1602.
39. Li X, Welch EB, Chakravarthy AB, et al. Statistical comparison of dynamic contrast-enhanced MRI pharmacokinetic models in human breast cancer. *Magn Reson Med*. 2012;68:261–271.
40. Li X, Welch EB, Arlinghaus LR, et al. A novel AIF tracking method and comparison of DCE-MRI parameters using individual and population-based AIFs in human breast cancer. *Phys Med Biol*. 2011;56:5753–5769.
41. Planey CR, Welch EB, Xu L, et al. Temporal sampling requirements for reference region modeling of DCE-MRI data in human breast cancer. *J Magn Reson Imaging*. 2009;30:121–134.

42. Atuegwu NC, Arlinghaus LR, Li X, et al. Parameterizing the logistic model of tumor growth by DW-MRI and DCE-MRI data to predict treatment response and changes in breast cancer cellularity during neoadjuvant chemotherapy. *Transl Oncol*. 2013;6:256–264.
43. Maes F, Collignon A, Vandermeulen D, et al. Multimodality image registration by maximization of mutual information. *IEEE Trans Med Imaging*. 1997;16:187–198.
44. Li X, Welch EB, Chakravarthy AB, et al. A novel AIF detection method and a comparison of DCE-MRI parameters using individual and population based AIFs in human breast cancer. *Phys Med Biol*. 2011;56:5753–5769.
45. Hanley JA, McNeil BJ. The meaning and use of the area under a receiver operating characteristic (ROC) curve. *Radiology*. 1982;143:29–36.
46. Perkins NJ, Schisterman EF. The inconsistency of "optimal" cutpoints obtained using two criteria based on the receiver operating characteristic curve. *Am J Epidemiol*. 2006;163:670–675.
47. Lehmann EL. Parametric versus nonparametrics: two alternative methodologies. *J Nonparametr Stat*. 2009;21:397–405.
48. Efron B, Tibshirani RJ. *An Introduction of the Bootstrap*. New York, NY: Chapman and Hall/CRC; 1993.
49. Cerussi AE, Tanamai VW, Hsiang D, et al. Diffuse optical spectroscopic imaging correlates with final pathological response in breast cancer neoadjuvant chemotherapy. *Phil Trans R Soc A*. 2011;369:4512–4530.
50. Padhani AR, Miles KA. Multiparametric imaging of tumor response to therapy. *Radiology*. 2010;256:348–364.
51. Hahn SY, Ko EY, Han BK, et al. Role of diffusion-weighted imaging as an adjunct to contrast-enhanced breast MRI in evaluating residual breast cancer following neoadjuvant chemotherapy. *Eur J Radiol*. 2014;83:283–288.
52. Jensen LR, Garzon B, Heldahl MG, et al. Diffusion-weighted and dynamic contrast-enhanced MRI in evaluation of early treatment effects during neoadjuvant chemotherapy in breast cancer patients. *J Magn Reson Imaging*. 2011;34:1099–1109.
53. Therasse P, Arbuck SG, Eisenhauer EA, et al. New guidelines to evaluate the response to treatment in solid tumors. European Organization for Research and Treatment of Cancer, National Cancer Institute of the United States, National Cancer Institute of Canada. *J Natl Cancer Inst*. 2000;92:205–216.
54. Eisenhauer EA, Therasse P, Bogaerts J, et al. New response evaluation criteria in solid tumours: revised RECIST guideline (version 1.1). *Eur J Cancer*. 2009;45:228–247.
55. Therasse P, Eisenhauer EA, Verweij J. RECIST revisited: a review of validation studies on tumour assessment. *Eur J Cancer*. 2006;42:1031–1039.
56. von Minckwitz G, Blohmer JU, Costa SD, et al. Response-guided neoadjuvant chemotherapy for breast cancer. *J Clin Oncol*. 2013;31:3623–3630.
57. Hylton NM, Blume JD, Bernreuter WK, et al. Locally advanced breast cancer: MR imaging for prediction of response to neoadjuvant chemotherapy—results from ACRIN 6657/I-SPY TRIAL. *Radiology*. 2012;263:663–672.
58. Loo CE, Straver ME, Rodenhuis S, et al. Magnetic resonance imaging response monitoring of breast cancer during neoadjuvant chemotherapy: relevance of breast cancer subtype. *J Clin Oncol*. 2011;29:660–666.
59. De Los Santos J, Bernreuter W, Keene K, et al. Accuracy of breast magnetic resonance imaging in predicting pathologic response in patients treated with neoadjuvant chemotherapy. *Clin Breast Cancer*. 2011;11:312–319.